Effect of the stiffness of interparticle bonds on properties of delocalized nonlinear vibrational modes in an fcc lattice

Rita I. Babicheva,[1] Alexander S. Semenov,[2] Stepan A. Shcherbinin,[3,4] Elena A. Korznikova,[4,5] Aleksey A. Kudreyko,[6] Priyanka Vivegananthan,[1] Kun Zhou,[1,*] and Sergey V. Dmitriev[4,7]

[1]*School of Mechanical and Aerospace Engineering, Nanyang Technological University, 50 Nanyang Avenue, Singapore 639798, Singapore*
[2]*Polytechnic Institute (Branch) in Mirny, North-Eastern Federal University, Tikhonova Street 5/1, Mirny 678170, Sakha Republic (Yakutia), Russia*
[3]*Peter the Great St. Petersburg Polytechnic University, Politekhnicheskaya Street 29, St. Petersburg 195251, Russia*
[4]*Institute of Molecule and Crystal Physics, Ufa Federal Research Centre of Russian Academy of Sciences, Oktyabrya Avenue 151, Ufa 450075, Russia*
[5]*Ufa State Aviation Technical University, Laboratory "Metals and Alloys under Extreme Impacts", Karl Marx Street 12, Ufa 450077, Russia*
[6]*Department of Medical Physics and Informatics, Bashkir State Medical University, Lenin Street 3, Ufa 450008, Russia*
[7]*Institute of Mathematics with Computing Centre, Ufa Federal Research Centre of Russian Academy of Sciences, Ufa 450008, Russia*

(Received 18 March 2022; accepted 6 May 2022; published 8 June 2022)

Delocalized nonlinear vibrational modes (DNVMs) supported in crystal lattices are exact solutions to the equations of motion of particles that are determined by the symmetry of the lattices. DNVMs exist for any vibration amplitudes and for any interparticle potentials. It is important to know how the properties of DNVMs depend on the parameters of interparticle potentials. In this work, we analyze the effect of the Morse potential stiffness on the properties of one-component DNVMs in a face-centered cubic (fcc) lattice. In particular, the frequencies, kinetic and potential energy, mechanical stress, and elastic constants of DNVMs in a large range of vibration amplitudes are considered. Frequency-amplitude dependency obtained for the Morse crystal is compared with that obtained earlier for copper by using the potentials of the many-body embedded atom method. The properties of DNVMs are mainly dictated by their symmetry and are less influenced by the interparticle potentials. It is revealed that at low and high stiffness of interparticle bonds, different sets of DNVMs have frequencies above the phonon band. This is important to predict the possible types of discrete breathers supported by the fcc lattice. The results obtained in the work enrich the understanding of the influence of interparticle potentials on the properties of the studied family of exact dynamic solutions.

DOI: 10.1103/PhysRevE.105.064204

I. INTRODUCTION

Large-amplitude spatially localized vibrational modes in defect-free nonlinear lattices, known as discrete breathers (DBs) or intrinsic localized modes, have attracted much research attention [1–3] since their discovery [4–6]. The existence of DBs in magnetic crystals has recently been proven [7]. However, there are fewer studies on the delocalized nonlinear vibrational modes (DNVMs), which were originally called bushes of nonlinear normal modes (BNNMs) [8–10]. Such modes are derived using group-theoretical methods that take into account only the symmetry of the lattice, and therefore they exist as exact solutions for any amplitudes and any laws of interparticle interaction.

BNNMs can be constructed for molecules by using their point symmetry [11] and for crystals by using space symmetry [12–15]. In crystals, DNVMs are spatially periodic short-wavelength modes that do not excite other vibrational modes even at high amplitudes.

DNVMs with n degrees of freedom are described by n coupled equations of motion and therefore called the n-component DNVMs or, in the original works, the n-dimensional BNNMs [8–10].

By now, DNVMs have been studied in various materials, for example, in nonlinear chains [12,16–19], carbyne [13], graphene [15,20–23], diamond [14], and face-centered cubic (fcc) and body-centered cubic (bcc) metals [17,24–28]. DNVMs with frequencies outside the phonon band of the lattice can be used for obtaining new types of DBs by superimposing a localizing function [20,25,29–32]. It has been revealed that DNVMs affect the elastic constants of nonlinear lattices [21,33], and the modulational instability of DNVMs with frequencies outside the phonon band results in the formation of chaotic DBs [29,34–43]. Recently, it has been demonstrated that DNVMs can be used to assess the accuracy of interatomic potentials [28].

Undoubtedly, such an interesting dynamic subject as DNVMs deserves careful study of various lattices. The existence of DNVMs as exact solutions is guaranteed by the lattice symmetry and, as mentioned above, does not depend on interparticle potentials. On the other hand, the DNVM frequency, energy, and their effect on lattice properties do depend on the potentials.

In this work, we analyze the effect of the stiffness of interparticle bonds on the DNVMs in an fcc lattice [28].

*Corresponding author; kzhou@ntu.edu.sg

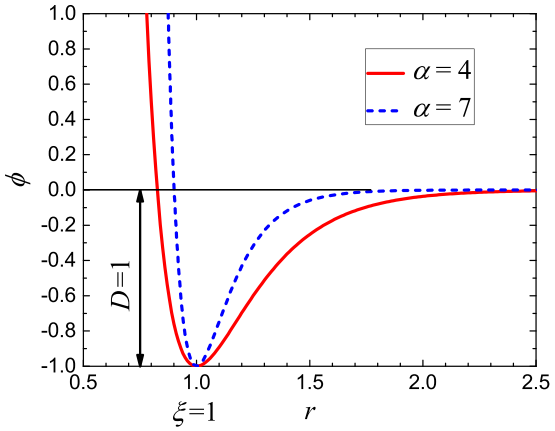

FIG. 1. Morse potential Eq. (1) for $\alpha = 4$ (the solid red line) and $\alpha = 7$ (the dashed blue line). The binding energy $D = 1$ and the equilibrium interparticle distance $\xi = 1$.

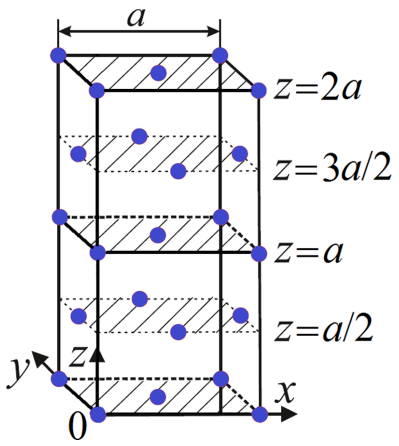

FIG. 2. Structure of the fcc lattice with the lattice parameter a. Two cubic lattice cells are shown, while the calculations use a block of $2 \times 2 \times 2$ cubic cells with four particles each, for a total of 32 particles.

The classical Morse potential [44,45] is used, which has one essential parameter: the bond stiffness.

Simulation details are described in Sec. II, including the initial conditions used to excite the one-component DNVMs of the fcc lattice, which were reported in Ref. [28]. Numerical results are presented in Sec. III. In particular, the frequency as the function of amplitude for all studied DNVMs is reported in Sec. III B, the energy of the DNVMs is discussed in Sec. III C, and stress components induced in the lattice by the DNVMs are summarized in Sec. III D. Section IV concludes the work and provides directions for future research.

II. SIMULATION METHOD

In this section, the fcc Morse crystal and its macroscopic characteristics are described, followed by one-component DNVMs as described in Ref. [28].

A. Morse crystal and its macroscopic parameters

The properties of DNVMs are analyzed with the use of the molecular dynamics method based on pairwise Morse interparticle potential [44,45]

$$\phi(r) = D[(1 - e^{-\alpha(r-\xi)})^2 - 1], \tag{1}$$

where ϕ is the potential energy of the interaction between two particles, r is the distance between the particles, D is the binding energy, ξ is the equilibrium distance between the particles, and α determines the bond stiffness. Dimensionless variables will be used in this study. For the particle mass, we set $m = 1$ using the appropriate unit of time. By choosing the suitable units for energy and distance, one can set $D = 1$ and $\xi = 1$. The effect of the remaining parameter on the properties of DNVMs will be analyzed further in detail. We will consider two values $\alpha = 4$ and $\alpha = 7$. The potential functions in Eq. (1) for these values are compared in Fig. 1. It can be seen that as α increases, the curvature of the potential near the minimum increases, and the potential becomes a short-range one. The cut-off radius $R_c = 10$ is used for both values of α. The equilibrium lattice parameter $a = 1.27478$ for $\alpha = 4$ and $a = 1.40208$ for $\alpha = 7$. As α increases, a tends to $\sqrt{2}$, and the interatomic distance $\rho = a/\sqrt{2}$ approaches 1.

The expansion of the Morse potential Eq. (1) in a Taylor series at $r = \xi$ reads

$$\phi(r) = D\Big[-1 + \alpha^2(r-\xi)^2 - \alpha^3(r-\xi)^3 + \frac{7}{6}\alpha^4(r-\xi)^4 - \cdots\Big]. \tag{2}$$

This shows that the coefficient in front of the harmonic term is proportional to α^2. The anharmonic part is an alternating series and its contribution increases with α. We conclude that an increase in α leads to an increase in the nonlinearity of the system. The influence of the potential stiffness parameter α on the properties of the DNVMs considered in this study is, on the other hand, the influence of the system's nonlinearity.

The fcc lattice with the lattice parameter a is shown in Fig. 2. As will become clear later, all DNVMs can be simulated by using a computational cell consisting of $2 \times 2 \times 2$ cubic translational cells with the fcc lattice, and the total number of particles is equal to 32. Periodic boundary conditions are applied.

The Hamiltonian of the fcc lattice is the sum of kinetic (K) and potential (P) energy

$$H = E_{\text{kin}} + E_{\text{pot}} = \frac{m}{2}\sum_i (\dot{\boldsymbol{r}}_i, \dot{\boldsymbol{r}}_i) + \sum_{i>j} \phi(|\boldsymbol{R}_{i,j}|), \tag{3}$$

where $\boldsymbol{r}_i = (r_{i,x}, r_{i,y}, r_{i,z})$ is the radius vector of the ith particle, with the overdot referring to the differentiation of the radius vector with respect to time, and $\boldsymbol{R}_{i,j} = \boldsymbol{r}_j - \boldsymbol{r}_i$.

The Hamilton's equations of motion derived from Eq. (3) are

$$\begin{aligned} m\ddot{r}_{i,x} &= -\sum_{i>j} F_{i,j} R_{i,j,x}, \\ m\ddot{r}_{i,y} &= -\sum_{i>j} F_{i,j} R_{i,j,y}, \\ m\ddot{r}_{i,z} &= -\sum_{i>j} F_{i,j} R_{i,j,z}, \end{aligned} \tag{4}$$

where

$$F_{i,j} = \frac{\phi'(|\boldsymbol{R}_{i,j}|)}{|\boldsymbol{R}_{i,j}|}. \tag{5}$$

A home-made computational code written in the C++ algorithmic language is developed for simulations. The Störmer symplectic method of the sixth order [46] with a time step of 0.001 is used to integrate the equations of motion in Eq. (4).

Components of the mechanical stress in the lattice can be calculated as follows:

$$\begin{aligned}
\sigma_{xx} &= -\frac{1}{V}\sum_{i>j} F_{i,j}R_{i,j,x}^2,\\
\sigma_{yy} &= -\frac{1}{V}\sum_{i>j} F_{i,j}R_{i,j,y}^2,\\
\sigma_{zz} &= -\frac{1}{V}\sum_{i>j} F_{i,j}R_{i,j,z}^2,\\
\tau_{xy} &= -\frac{1}{V}\sum_{i>j} F_{i,j}R_{i,j,x}R_{i,j,y},\\
\tau_{xz} &= -\frac{1}{V}\sum_{i>j} F_{i,j}R_{i,j,x}R_{i,j,z},\\
\tau_{yz} &= -\frac{1}{V}\sum_{i>j} F_{i,j}R_{i,j,y}R_{i,j,z},
\end{aligned} \tag{6}$$

where V is the computational cell volume.

The stress components are related to the strain components according to Hooke's law

$$\begin{bmatrix}\sigma_{xx}\\ \sigma_{yy}\\ \sigma_{zz}\\ \tau_{xy}\\ \tau_{xz}\\ \tau_{yz}\end{bmatrix} = \begin{bmatrix}C_{11} & C_{12} & C_{13} & C_{14} & C_{15} & C_{16}\\ C_{21} & C_{22} & C_{23} & C_{24} & C_{25} & C_{26}\\ C_{31} & C_{32} & C_{33} & C_{34} & C_{35} & C_{36}\\ C_{41} & C_{42} & C_{43} & C_{44} & C_{45} & C_{46}\\ C_{51} & C_{52} & C_{53} & C_{54} & C_{55} & C_{56}\\ C_{61} & C_{62} & C_{63} & C_{64} & C_{65} & C_{66}\end{bmatrix}\begin{bmatrix}\varepsilon_{xx}\\ \varepsilon_{yy}\\ \varepsilon_{zz}\\ \gamma_{xy}\\ \gamma_{xz}\\ \gamma_{yz}\end{bmatrix}, \tag{7}$$

where $C_{ij} = C_{ji}$ are the stiffness constants. Only the diagonal stiffness constants will be analyzed and are given as

$$\begin{aligned}
C_{11} &= \frac{1}{V}\sum_{i>j} G_{i,j}R_{i,j,x}^4,\\
C_{22} &= \frac{1}{V}\sum_{i>j} G_{i,j}R_{i,j,y}^4,\\
C_{33} &= \frac{1}{V}\sum_{i>j} G_{i,j}R_{i,j,z}^4,\\
C_{44} &= \frac{1}{V}\sum_{i>j} G_{i,j}R_{i,j,x}^2R_{i,j,y}^2,\\
C_{55} &= \frac{1}{V}\sum_{i>j} G_{i,j}R_{i,j,x}^2R_{i,j,z}^2,\\
C_{66} &= \frac{1}{V}\sum_{i>j} G_{i,j}R_{i,j,y}^2R_{i,j,z}^2,
\end{aligned} \tag{8}$$

where

$$G_{i,j} = \frac{\phi_n''(|\boldsymbol{R}_{i,j}|)}{|\boldsymbol{R}_{i,j}|^2} - \frac{\phi_n'(|\boldsymbol{R}_{i,j}|)}{|\boldsymbol{R}_{i,j}|^3}. \tag{9}$$

Excitation of DNVMs leads to a periodic change of internal stress components and elastic constants. Therefore for the analysis, the stress components and stiffness constants averaged over the oscillation period will be considered as

$$\langle\sigma_{ij}\rangle = \frac{1}{T}\int_0^T \sigma_{ij}(t)dt, \quad \langle C_{ij}\rangle = \frac{1}{T}\int_0^T C_{ij}(t)dt. \tag{10}$$

Similarly, the kinetic energy and potential energy of the computational cell per particle are averaged over the oscillation period as

$$\langle E_{\rm kin}\rangle = \frac{1}{NT}\int_0^T E_{\rm kin}(t)dt, \ \langle E_{\rm pot}\rangle = \frac{1}{NT}\int_0^T E_{\rm pot}(t)dt, \tag{11}$$

where $N = 32$ is the number of particles in the computational cell.

The initial conditions are set to excite one of the twelve one-component DNVMs, as explained in Sec. II B.

B. One-component DNVMs in the fcc lattice

DNVMs for the fcc lattice have been obtained in the earlier work [28] by using the theory of BNNMs [8–10]. Here, we reproduce them for the sake of completeness and clearness.

DNVMs can be excited by applying the initial displacement patterns presented in Fig. 3 with zero initial velocities. In the one-component DNVMs considered in this study, all the initial displacement vectors are either zero or having the same magnitude of A, which is the amplitude of the DNVMs. Displacement components Δx and Δy are shown in the x-y plane by arrows while Δz by dots (positive), crosses (negative), or empty circles (zero). All nonzero components of the displacements have the same magnitude. If a particle has only one nonzero component of the displacement vector, then it is equal to A (DNVMs 2, 4, 7, and 10). If a particle has two nonzero components of the displacement vector, then they are equal to $A/\sqrt{2}$ (DNVMs 5, 8, 9, and 12). For a particle having three nonzero components of the displacement vector, they are equal to $A/\sqrt{3}$ (DNVMs 1, 3, 6, and 11).

The computational cell for DNVMs 1, 2, and 3 includes $2\times2\times2$ cubic translational cells with the fcc lattice. For all other DNVMs, it has a spatial period equal to one fcc translational cell.

C. Simulation protocol

By exciting a DNVM and integrating the equations of motion in Eq. (4), we find the time evolution of the displacement components $\Delta x(t)$, $\Delta y(t)$, and $\Delta z(t)$. Since all DNVMs are exactly periodic in time solutions, it is sufficient to integrate over one oscillation period. Thus the temporal period of the DNVM, T, and DNVM frequency $\omega = 2\pi/T$ can be defined. Further, the stress components and elastic constants, as well as the kinetic and potential energy of the computational cell per particle, averaged over a period were calculated using Eqs. (10) and (11).

Note that for not too small oscillation amplitudes, DNVMs are modulationally unstable [29,34–42]. However, this

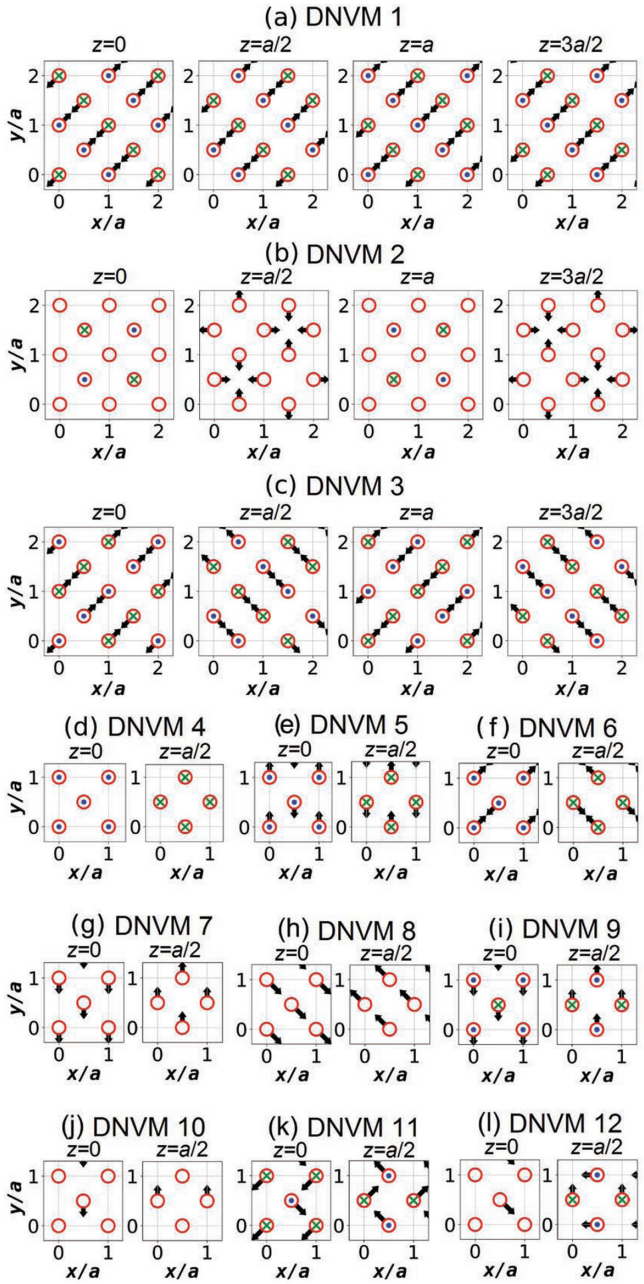

FIG. 3. Initial particle displacements used for excitation of DNVMs from 1 to 12. All particles have zero initial velocities. Displacements are shown in the particle planes parallel to the x-y plane with the z coordinate indicated for each panel. All non-zero displacement vectors have the same length A. Displacements Δx and Δy are shown in the x, y plane by arrows while Δz by dots (positive), crosses (negative) or empty circles (zero). All nonzero components of displacements have the same magnitude.

instability does not manifest itself during the several oscillation periods modeled in this study.

III. NUMERICAL RESULTS

In this section, we analyze the dispersion curves obtained for the fcc lattice with DNVMs, and discuss the effect of DNVMs on the energy and mechanical responses.

TABLE I. Maximal phonon frequencies at the two points of the first Brillouin zone and equilibrium interatomic distances ρ for different values of the potential stiffness parameter α.

α	$\omega_{\max}$ at $q_x = q_y = q_z = 0$	$\omega_{\max}$ at $q_x = q_y = q_z = \pi$	$\rho = a/\sqrt{2}$
4	26.16	26.62	0.9014073
5	25.81	25.75	0.9611802
6	27.68	27.48	0.9824828
7	30.43	30.22	0.9914215

A. Phonon dispersion curves for the fcc lattice

It is important to know the location of the DNVM frequency with respect to the phonon spectrum of the fcc lattice. In particular, DNVMs with frequencies above the phonon band are of interest for the study of DBs [20,25,29–32]. In the current work, the frequency spectrum of low-amplitude phonon waves is calculated.

Cubic translational cells of the fcc lattice are numbered by indices m, n, and k. Each cell contains four particles. The eigenproblem for finding the normal vibrational modes was formulated by considering the eigenvector with 12 components, which are the displacements of particles in the (m, n, k)-th translational cell: $\mathbf{e} = (\Delta x_1, \Delta y_1, \Delta z_1, ..., \Delta x_4, \Delta y_4, \Delta z_4)$.

Phonon waves are taken in the standard form

$$\mathbf{w}_n = A\mathbf{e}\exp[i(q_x m + q_y n + q_z k - \omega t)], \qquad (12)$$

where A is the amplitude, $\mathbf{e}$ is the normalized eigenvector ($|\mathbf{e}| = 1$), i is the imaginary unit, $q_x, q_y, q_z \in [-\pi, \pi]$ are dimensionless wave numbers, and ω is the frequency. By substituting Eq. (12) into the linearized equations of motion Eq. (4), a 12-dimensional eigenvalue problem was obtained, which is solved by the Jacobi algorithm [47].

By solving the eigenvalue problem for a set of wave numbers, one can obtain the dispersion curves shown in Fig. 4. All dispersion curves are double-folded because the translational unit cell in our calculations is not a primitive translation cell. The dispersion curves are presented for the three lines in the first Brillouin zone: (a) $q_x \in [0, \pi]$, $q_y = q_z = 0$; (b) $q_x = q_y \in [0, \pi]$, $q_z = 0$; and (c) $q_x = q_y = q_z \in [0, \pi]$. In other words, we discuss the phonon waves propagating along the (a) [001], (b) [011], and (c) [111] crystallographic directions.

Note that for the double-folded dispersion curves, shown in Fig. 4, the point $q_x = q_y = q_z = 0$ is the Γ point only for curves with zero frequency. For curves with nonzero frequency, the point $q_x = q_y = q_z = 0$ corresponds to the boundary of the first Brillouin zone. The point $q_x = q_y = q_z = \pi$ is in the middle between the Γ-point and zone boundary.

There are three branches of the dispersion curves for the longitudinal wave (L) and the two transverse waves (T_1, T_2) having different polarization. It can be seen that the dispersion curves for T_1 and T_2 in Figs. 4(a) and 4(c) coincide, while they are different in Fig. 4(b).

The phonons with the maximal frequency can have different wave numbers depending on the stiffness of the interparticle potential α, as seen in Table I. For $\alpha = 4$, the maximum is achieved at $q_x = q_y = q_z = 0$, while for $\alpha \geqslant 5$,

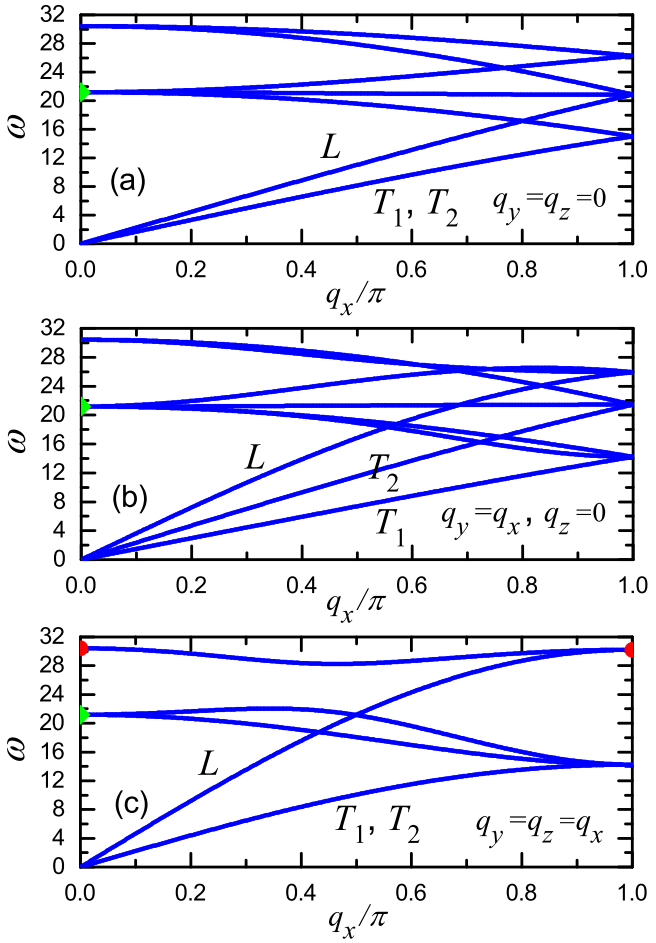

FIG. 4. Dispersion curves for the fcc crystal along the crystallographic directions: (a) [001], (b) [011], and (c) [111]. The potential stiffness parameter α is 7.

the maximum is reached at $q_x = q_y = q_z = \pi$. These two points are marked by red circles in Fig. 4(c).

B. Frequency-amplitude dependency for DNVMs

Frequency-amplitude dependency for DNVMs in the Morse lattice is given in Figs. 5(a) and 5(b) for the potential stiffness parameter $\alpha = 4$ and 7, respectively. For comparison, the result for fcc copper obtained in Ref. [28] using the interatomic potential of the many-body embedded atom method (EAM) by Zhou *et al.* [48] is presented in Fig. 5(c).

In Figs. 5(a) and 5(b), the dotted horizontal lines show the maximal phonon frequencies. It may seem that DNVMs 1 to 6 have the same frequency as the maximum phonon frequency at small amplitudes, while it is not true. The first three DNVMs in the limit of small amplitudes become the phonon with the wave numbers $q_x = q_y = q_z = \pi$, while DNVMs 4 to 6 become the phonon with the wave numbers $q_x = q_y = q_z = 0$. Thus, according to Table I, DNVMs 1 to 3 for $\alpha = 4$ diverge from the upper edge of the phonon band at small amplitudes, but DNVMs 4 to 6 lie within the phonon band, although they are close to the upper edge. For $\alpha = 7$, the situation is the opposite (see Table I) that at low amplitudes, DNVMs 4 to 6 have higher frequencies than DNVMs 1 to 3.

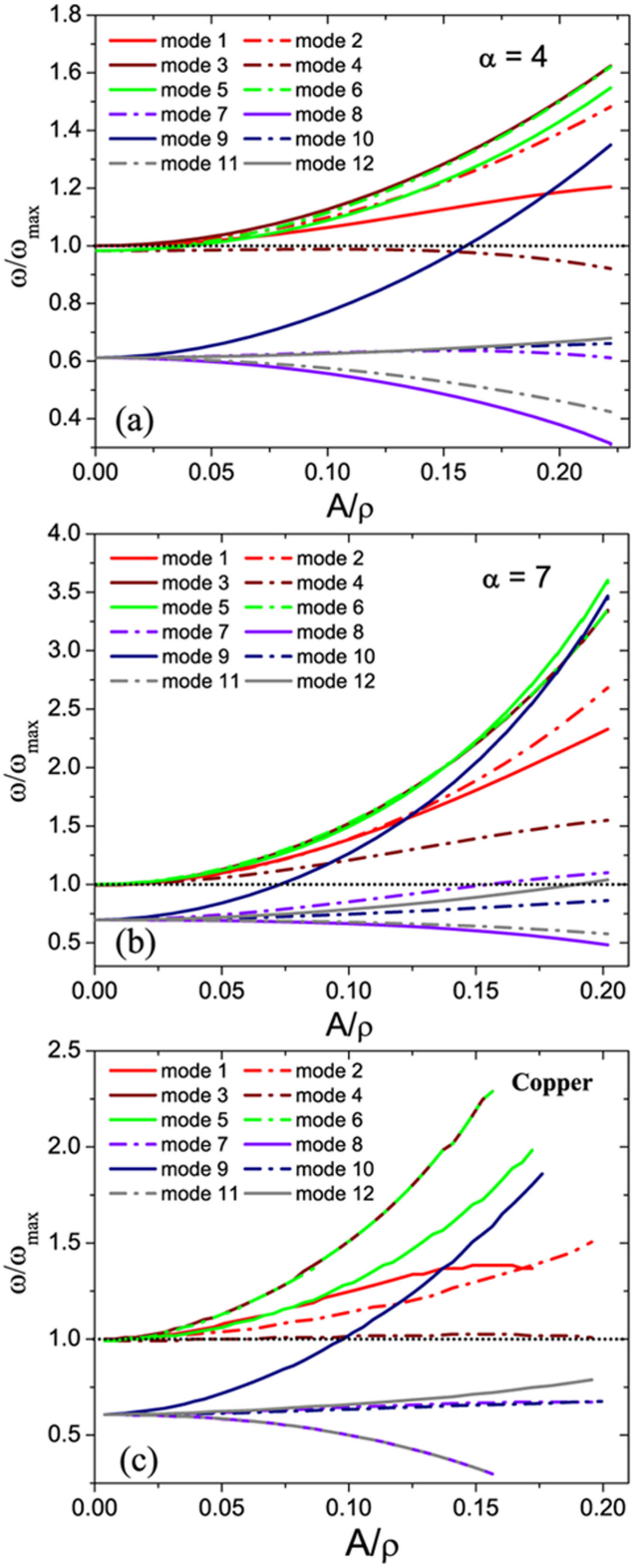

FIG. 5. Frequency-amplitude dependency for 12 DNVMs in the Morse lattice for (a) α=4 and (b) α=7. The horizontal dotted lines indicate the corresponding maximum frequency of the phonon spectrum. (c) Frequency-amplitude dependency for 12 DNVMs in fcc copper obtained in Ref. [28] using the EAM interatomic potentials developed by Zhou *et al.* [48]. The DNVM amplitude is normalized to the interparticle distance ρ and the DNVM frequency is normalized to the maximal phonon frequency $\omega_{\max}$.

Note that the frequencies for DNVMs 7 to 12 start at the same point well below the upper edge of the phonon band. In the limit of small amplitudes, these modes become phonons with the wave numbers $q_x = q_y = q_z = 0$, as indicated in Figs. 4(a)–4(c) by the green triangles.

As the amplitude increases, some DNVMs exhibit a hard-type anharmonicity, that is, an increase in the frequency with the amplitude, while other modes exhibit a soft-type anharmonicity where the frequency decreases with the amplitude. Some modes show an increase in the frequency with the amplitude at moderate amplitudes and demonstrate a decrease in the frequency only at higher amplitudes, e.g., DNVM 7 for $\alpha = 4$ in Fig. 5(a).

By comparing Figs. 5(a) and 5(b), it can be concluded that for a larger α value, the frequency increases with the amplitude more quickly or decreases more slowly. In particular, the frequency of DNVM 4 in Fig. 5(a) decreases but in Fig. 5(b) increases with the amplitude A.

The frequency-amplitude dependency for copper, as shown in Fig. 5(c), are closer to those obtained for the Morse lattice with $\alpha = 4$, rather than $\alpha = 7$. Indeed, the frequencies of DNVM 1 and DNVM 4 in Fig. 5(a) show a tendency to soften at a large amplitude, similar to what is observed for copper. In addition, in copper, DNVMs 1 to 3 have higher frequencies at low amplitudes than DNVMs 4 to 6, as in the case of the Morse lattice with $\alpha = 4$.

In general, the behavior of the frequency-amplitude dependency is mainly determined by the symmetry of the DNVMs, and not by the interatomic potentials, since the results for the pairwise Morse potential with significantly different parameter α, and even for the many-body EAM potential, have much in common [cf. Figs. 5(a) and 5(c)].

C. Energy of DNVMs

In linear lattices, the time-averaged kinetic energy and potential energy are equal. The deviation of these two types of energy from each other characterizes the anharmonicity of nonlinear oscillations.

In Fig. 6, the kinetic and potential energy of the computational cell per atom averaged over a period of oscillation, according to Eq. (11), is presented as functions of the amplitude for the 12 considered DNVMs. The angle brackets are omitted for brevity. The results for $\alpha = 4$ ($\alpha = 7$) are plotted by the solid (dash-dotted) lines. The kinetic (potential) energy is shown by the black (red) curves.

Most DNVMs have higher kinetic energy than potential energy, with the exception of DNVMs 8 and 11. This result correlates with the frequency-amplitude dependency for DNVMs. As seen in Fig. 5, DNVMs 8 and 11 exhibit soft anharmonicity. Moreover, DNVMs with rapidly growing frequency-amplitude curves show a much faster increase in energy with the amplitude, as seen in the panels for DNVMs 3, 5, 6, and 9 in Fig. 6. The DNVMs with soft anharmonicity have lower energy, e.g., DNVMs 8, 10, 11, and 12.

D. Mechanical response of the lattice to DNVM excitation

Since the lattice is constrained by periodic boundary conditions, excitation of a DNVM leads to the appearance of internal mechanical stress. Excitation of a DNVM affects also the stiffness of the lattice. The stress and stiffness constants fluctuate over time with a period equal to half the period of the DNVM, and we analyze the values averaged over period by Eq. (10).

The dependency of the time-averaged stress components and stiffness constants on the DNVM amplitude are shown in Figs. 7 and 8, respectively, by the solid (dash-dotted) lines for $\alpha = 4$ ($\alpha = 7$). The angle brackets indicating average values are omitted for brevity.

All curves in Figs. 7 and 8 start growing with a zero derivative, which means that the appearance of stress and change of the stiffness constants due to DNVMs are nonlinear effects that are not observed at low amplitudes.

The symmetry of DNVMs determines the number of unequal stress components and the relationship between different stiffness constants.

Comparison of Fig. 7 with Fig. 8 reveals a correlation between the stress components and stiffness constants. For example, for high-symmetry DNVMs 1, 2, 3, 6, 11, and 12, the normal and shear stresses are equal, i.e., $\sigma_{xx} = \sigma_{yy} = \sigma_{zz}$ and $\tau_{xy} = \tau_{xz} = \tau_{yz}$; and for the stiffness constants, the equalities $C_{11} = C_{22} = C_{33}$ and $C_{44} = C_{55} = C_{66}$ are satisfied. Note that C_{ii} characterizes the stiffness in relation to tension-compression for $i = 1$, 2, and 3 and in relation to shear for $i = 4$, 5 and 6.

For other modes with lower symmetry, there remains the correlation between the normal stress components σ_{xx}, σ_{yy}, σ_{zz} and elastic constants C_{11}, C_{22}, and C_{33}. In particular, for DNVM 4, $\sigma_{xx} = \sigma_{yy} \neq \sigma_{zz}$ and $C_{11} = C_{22} \neq C_{33}$. For DNVM 5, $\sigma_{xx} \neq \sigma_{yy} = \sigma_{zz}$ and $C_{11} \neq C_{22} = C_{33}$. For DNVM 7, $\sigma_{xx} \neq \sigma_{yy} \neq \sigma_{zz}$ and $C_{11} \neq C_{22} \neq C_{33}$. For DNVM 8, $\sigma_{xx} = \sigma_{yy} \neq \sigma_{zz}$ and $C_{11} = C_{22} \neq C_{33}$. For DNVM 9, $\sigma_{xx} \neq \sigma_{yy} = \sigma_{zz}$ and $C_{11} \neq C_{22} = C_{33}$. For DNVM 10, $\sigma_{xx} = \sigma_{zz} \neq \sigma_{yy}$ and $C_{11} = C_{33} \neq C_{22}$.

On the other hand, for low-symmetry DNVMs, the relationship between the shear stress components does not always correlate with the stiffness constants, because in some cases, the stiffness constants may be different, while the shear stress components are all zero. In fact, for DNVMs 4, 5, 9, and 10, $\tau_{xy} = \tau_{xz} = \tau_{yz} = 0$, but among C_{44}, C_{55}, and C_{66}, only two of the stiffness constants are equal. For DNVMs 7, $\tau_{xy} = \tau_{xz} = \tau_{yz} = 0$, but C_{44}, C_{55} and C_{66} are all different.

For DNVM 8, $C_{44} \neq C_{55} = C_{66}$ and $\tau_{xy} \neq \tau_{xz} = \tau_{yz}$. The correlation between shear stress components and elastic constants is observed only in this case.

Most of the DNVMs produce positive (compressive) normal stress. The exceptions are low-symmetry DNVMs 7 and 9 with a small negative σ_{xx} component. A fast growth of normal stress and elastic constants with the DNVM amplitude is observed for DNVMs 3, 5, 6, and 9. All these modes demonstrate strong hard-type anharmonicity, i.e., a rapid increase in the frequency with the amplitude, as seen in Fig. 5. DNVMs 8, 10, 11, and 12 demonstrating soft-type anharmonicity or a slow rise in the frequency with the amplitude also exhibit a slow increase in normal stress and elastic constants with the amplitude.

IV. CONCLUSIONS AND FUTURE RESEARCH DIRECTIONS

In the current work, the effects of the potential stiffness parameter α on the various properties of 12 one-component

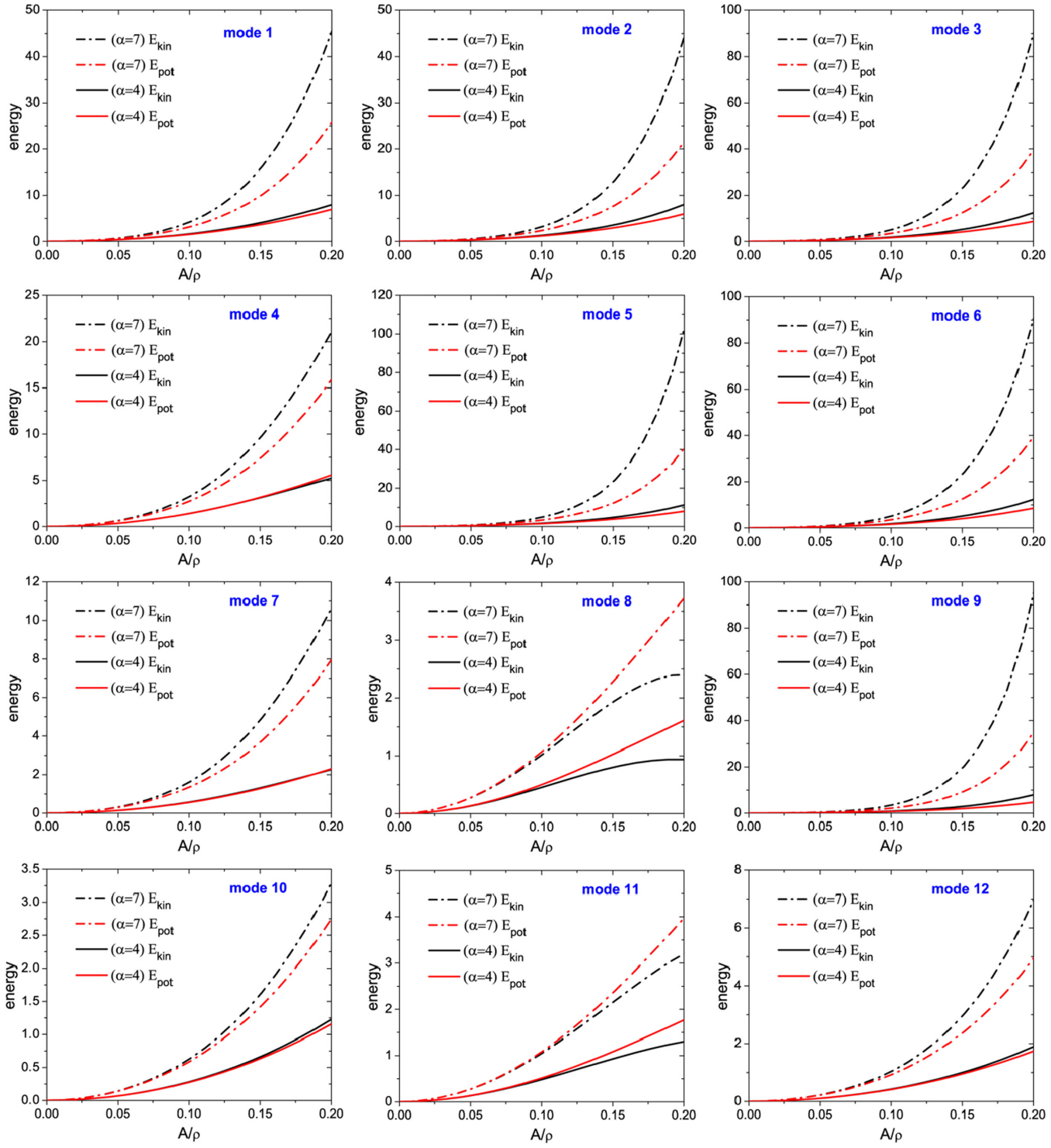

FIG. 6. Kinetic and potential energy of the computational cell per atom averaged over a period of oscillation as functions of amplitude for the 12 DNVMs (angle brackets are omitted for brevity). The results for $\alpha = 4$ ($\alpha = 7$) are plotted by the solid (dash-dotted) lines. The kinetic (potential) energy is shown by the black (red) curves.

DNVMs in the fcc Morse lattice (see Fig. 3) reported earlier in [28] are analyzed. More specifically, the frequency-amplitude dependency of DNVMs (Fig. 5) related to the phonon dispersion curves (Fig. 4), time-averaged kinetic and potential energy of the computational cell per atom (Fig. 6), and time-averaged stress components (Fig. 7) and stiffness constants (Fig. 8) induced by the DNVMs are systematically studied. DNVMs with large amplitudes affect the macroscopic characteristics of the lattice due to the anharmonicity and asymmetry of the Morse potential.

It is found that only three DNVMs have frequencies above the phonon band for any DNVM amplitude, and the other

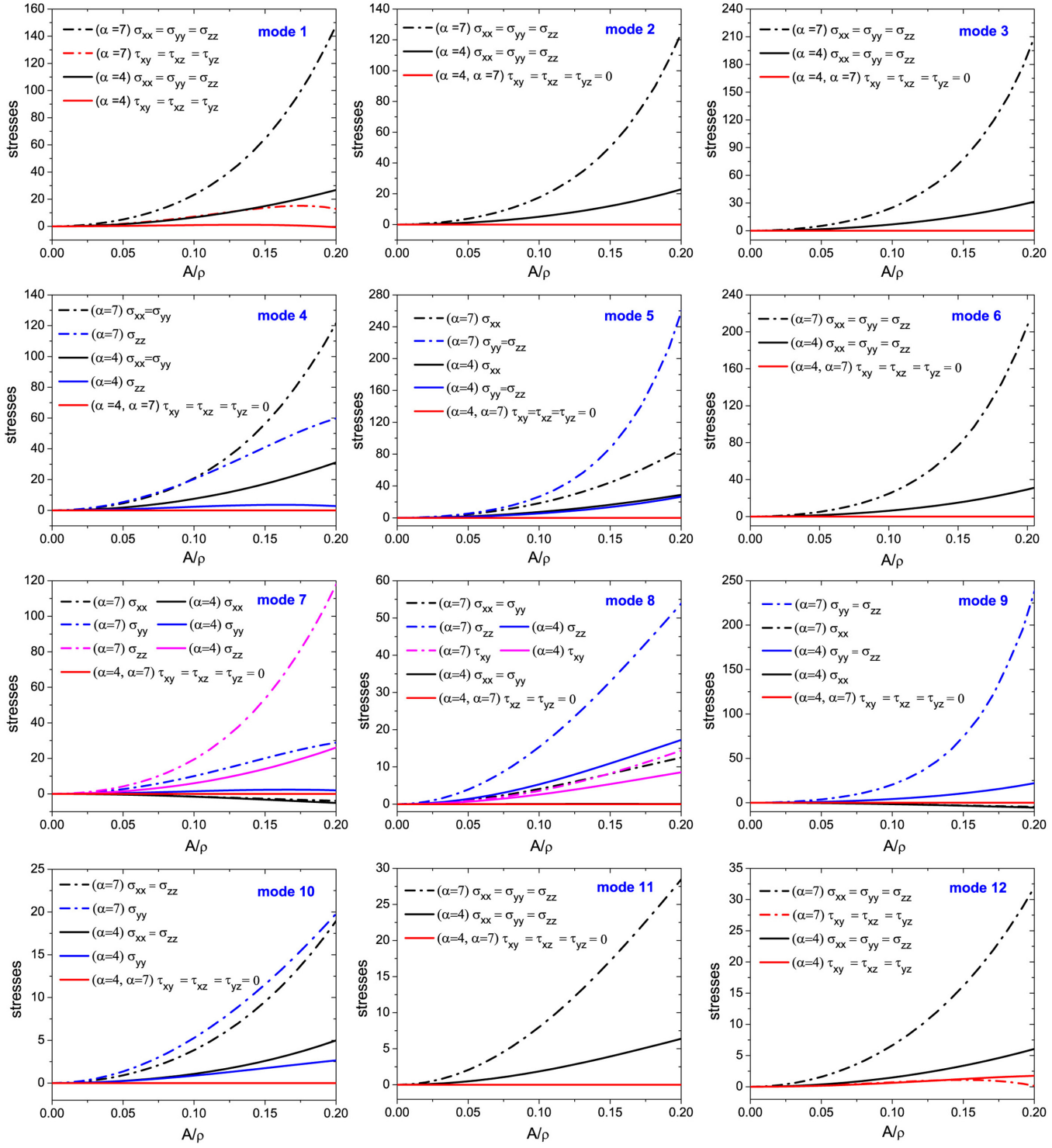

FIG. 7. Stress components averaged over a period of oscillation as functions of amplitude for the 12 DNVMs (angle brackets are omitted for brevity). The results for $\alpha = 4$ ($\alpha = 7$) are plotted by the solid (dash-dotted) lines.

modes have different results for different values of the potential stiffness parameter α. In particular, for $\alpha = 4$, DNVMs 1 to 3 have frequencies above the phonon band, while for $\alpha \geqslant 5$, this is true for DNVMs 4 to 6. However, the difference between frequencies of these modes at small amplitudes is very small, as shown in Table I.

This finding demonstrates that for different interparticle stiffness parameter values, different DNVMs have frequencies above the phonon band, which is of great importance to the analysis of possible types of DBs in fcc crystals. Note that different types of DBs can be obtained by superimposing localization functions on DNVMs that have frequencies outside the phonon band [27,32,49]. The obtained results indicate that in crystals with relatively soft interatomic bonds, DBs can be obtained using DNVMs 1 to 3, while for crystals with hard bonds, DBs can be obtained using DNVMs 4 to 6. Since

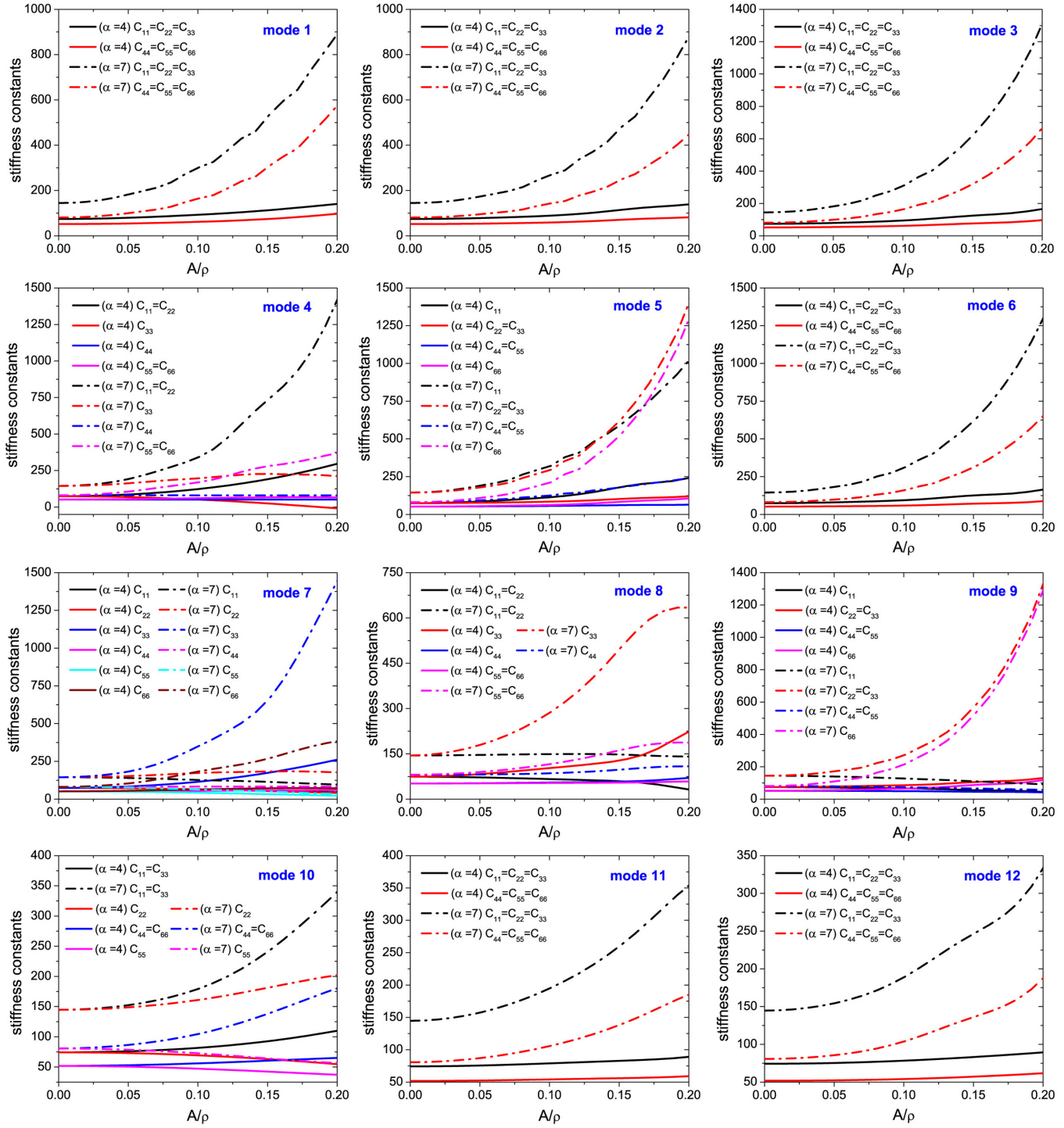

FIG. 8. Stiffness constants averaged over a period of oscillation as functions of amplitude for the 12 DNVMs (angle brackets are omitted for brevity). The results for $\alpha = 4$ ($\alpha = 7$) are plotted by the solid (dash-dotted) lines.

the difference between the frequencies of DNVMs 1 to 3 and DNVMs 4 to 6 at low amplitudes is very small, it is expected that all six DNVMs can create DBs with not too small amplitudes. This assumption will be analyzed in future study.

Analysis of the time-averaged kinetic and potential energy of DNVMs, as seen in Fig. 6, has revealed that the kinetic energy is greater than the potential energy, except for DNVMs 8 and 11. This can be explained by the soft anharmonicity of DNVMs 8 and 11, as seen in Fig. 5. DNVMs 3, 5, 6, and 9 with rapidly growing frequency-amplitude curves show a fast increase in the energy with the amplitude, as exhibited in Fig. 6, while DNVMs 8, 10, 11, and 12 with soft anharmonicity have lower energy.

The mechanical response of the lattice also correlates with the frequency-amplitude dependency of DNVMs. Most of the DNVMs produce positive (compressive) normal stress. The exceptions are low-symmetry DNVMs 7 and 9 with

a small negative σ_{xx} component. A fast growth of normal stress and elastic constants with the DNVM amplitude is observed for DNVMs 3, 5, 6, and 9, which demonstrates strong hard anharmonicity, as seen in Fig. 5. DNVMs exhibiting soft anharmonicity or a slow rise in the frequency with the amplitude also exhibit a slow increase in normal stress and elastic constants with the amplitude, e.g., DNVMs 8, 10, 11, and 12.

Chaotic DBs appear in the lattices as a result of the modulational instability of DNVMs with frequencies outside the phonon band [34–43]. The current study shows that DNVMs 1 to 6 are good candidates for creating chaotic DBs, and this should be verified in future work.

DNVMs exist as exact solutions for any type of interatomic interactions and for any amplitude. We believe that the DNVM frequency response obtained from *ab initio* calculations for various fcc metals can be very useful to fit interatomic potentials for molecular dynamics simulations. The DNVM dynamics can be modeled by using a small computational cell, and only a few oscillation periods are required to find the oscillation frequency, which is important for replacing the computationally demanding *ab initio* calculations.

Here, only one-component DNVMs are analyzed. In the next work, two-component DNVMs will be considered. Linear systems are also of interest because they can exhibit nontrivial dynamics and describe physically meaningful systems [50–52].

This work contributes to a deeper understanding of the nonlinear dynamics of the fcc lattice and opens a way for the study of related DBs.

ACKNOWLEDGMENTS

The work of S.S. (derivation of DNVMs) and S.D. (discussion, writing the manuscript) is funded by the Russian Science Foundation (Grant Reference No. 21-12-00229). E.K. (discussion of the results) is grateful for the financial support of Council on Grants of the President of the Russian Federation (Grant Reference No. NSh 4320.2022.1.2). The work is also supported by the Ministry of Science and Higher Education of the Russian Federation within the framework of the state assignment of Ufa State Aviation Technical University, the youth research laboratory "Metals and Alloys under Extreme Impacts" (Agreement No. 075-03-2022-318/1).

[1] S. Flach and C. R. Willis, Discrete breathers, Phys. Rep. **295**, 181 (1998).

[2] S. Flach and A. V. Gorbach, Discrete breathers—Advances in theory and applications, Phys. Rep. **467**, 1 (2008).

[3] S. V. Dmitriev, E. A. Korznikova, J. A. Baimova, and M. G. Velarde, Discrete breathers in crystals, Phys. Usp. **59**, 446 (2016).

[4] A. S. Dolgov, On the localization of vibrations in a nonlinear crystal structure, Fiz. Tve. Tela **28**, 1641 (1986) [Sov. Phys. Solid State **28**, 907 (1986)].

[5] A. J. Sievers and S. Takeno, Intrinsic Localized Modes in Anharmonic Crystals, Phys. Rev. Lett. **61**, 970 (1988).

[6] J. B. Page, Asymptotic solutions for localized vibrational modes in strongly anharmonic periodic systems, Phys. Rev. B **41**, 7835 (1990).

[7] I. G. Bostrem, E. G. Ekomasov, J. Kishine, A. S. Ovchinnikov, and V. E. Sinitsyn, Dark discrete breather modes in a monoaxial chiral helimagnet with easy-plane anisotropy, Phys. Rev. B **104**, 214420 (2021).

[8] V. P. Sakhnenko and G. M. Chechin, Symmetrical selection rules in nonlinear dynamics of atomic systems, Dokl. Akad. Nauk **330**, 308 (1993) [Phys. Dokl. **38**, 219 (1993)].

[9] V. P. Sakhnenko and G. M. Chechin, Groups of modes and normal oscillations for nonlinear dynamical systems with discrete symmetry, Dokl. Akad. Nauk **338**, 42 (1994) [Dokl. Math. **39**, 625 (1994)].

[10] G. M. Chechin and V. P. Sakhnenko, Interactions between normal modes in nonlinear dynamical systems with discrete symmetry. Exact results, Phys. D (Amsterdam, Neth.) **117**, 43 (1998).

[11] G. M. Chechin, D. S. Ryabov, and S. A. Shcherbinin, Nonlinear normal mode interactions in the SF_6 molecule studied with the aid of density functional theory, Phys. Rev. E **92**, 012907 (2015).

[12] A. V. Savin, I. R. Sunagatova, and S. V. Dmitriev, Rotobreathers in a chain of coupled elastic rotators, Phys. Rev. E **104**, 034207 (2021).

[13] G. M. Chechin, D. A. Sizintsev, and O. A. Usoltsev, Nonlinear atomic vibrations and structural phase transitions in strained carbon chains, Comput. Mater. Sci. **138**, 353 (2017).

[14] G. M. Chechin, D. S. Ryabov, and S. A. Shcherbinin, Large-amplitude periodic atomic vibrations in diamond, J. Micromechan. Mol. Phys. **03**, 1850002 (2018).

[15] G. M. Chechin, D. S. Ryabov, and S. A. Shcherbinin, Large-amplitude in-plane atomic vibrations in strained graphene monolayer: Bushes of nonlinear normal modes, Lett. Mater. **7**, 367 (2017).

[16] G. M. Chechin, D. S. Ryabov, and K. G. Zhukov, Stability of low-dimensional bushes of vibrational modes in the Fermi-Pasta-Ulam chains, Phys. D (Amsterdam, Neth.) **203**, 121 (2005).

[17] O. V. Bachurina, Linear discrete breather in fcc metals, Comput. Mater. Sci. **160**, 217 (2019).

[18] M. Singh, A. Y. Morkina, E. A. Korznikova, V. I. Dubinko, D. A. Terentiev, D. Xiong, O. B. Naimark, V. A. Gani, and S. V. Dmitriev, Effect of discrete breathers on the specific heat of a nonlinear chain, J. Nonlinear Sci. **31**, 12 (2021).

[19] E. A. Korznikova, A. Y. Morkina, M. Singh, A. M. Krivtsov, V. A. Kuzkin, V. A. Gani, Y. V. Bebikhov, and S. V. Dmitriev, Effect of discrete breathers on macroscopic properties of the Fermi-Pasta-Ulam chain, Eur. Phys. J. B **93**, 123 (2020).

[20] E. Barani, I. P. Lobzenko, E. A. Korznikova, E. G. Soboleva, S. V. Dmitriev, K. Zhou, and A. M. Marjaneh, Transverse discrete breathers in unstrained graphene, Eur. Phys. J. B **90**, 38 (2017).

[21] E. A. Korznikova, S. A. Shcherbinin, D. S. Ryabov, G. M. Chechin, E. G. Ekomasov, E. Barani, K. Zhou, and S. V. Dmitriev, Delocalized nonlinear vibrational modes in graphene: Second harmonic generation and negative pressure, Phys. Status Solidi (B) **256**, 1800061 (2019).

[22] S. A. Shcherbinin, M. N. Semenova, A. S. Semenov, E. A. Korznikova, G. M. Chechin, and S. V. Dmitriev, Dynamics of a three-component delocalized nonlinear vibrational mode in graphene, Phys. Solid State **61**, 2139 (2019).

[23] D. U. Abdullina, M. N. Semenova, A. S. Semenov, E. A. Korznikova, and S. V. Dmitriev, Stability of delocalized nonlinear vibrational modes in graphene lattice, Eur. Phys. J. B **92**, 249 (2019).

[24] O. V. Bachurina and A. A. Kudreyko, Two-dimensional discrete breathers in fcc metals, Comput. Mater. Sci. **182**, 109737 (2020).

[25] O. V. Bachurina, Plane and plane-radial discrete breathers in fcc metals, Model. Simul. Mater. Sci. **27**, 055001 (2019).

[26] O. V. Bachurina, R. T. Murzaev, and D. V. Bachurin, Molecular dynamics study of two-dimensional discrete breather in nickel, J. Micromechan. Mol. Phys. **4**, 1950001 (2019).

[27] K. A. Krylova, I. P. Lobzenko, A. S. Semenov, A. A. Kudreyko, and S. V. Dmitriev, Spherically localized discrete breathers in bcc metals V and Nb, Comput. Mater. Sci. **180**, 109695 (2020).

[28] S. A. Shcherbinin, K. A. Krylova, G. M. Chechin, E. G. Soboleva, and S. V. Dmitriev, Delocalized nonlinear vibrational modes in fcc metals, Commun. Nonlinear Sci. **104**, 106039 (2022).

[29] K. Ikeda, Y. Doi, B.-F. Feng, and T. Kawahara, Chaotic breathers of two types in a two-dimensional Morse lattice with an on-site harmonic potential, Phys. D (Amsterdam, Neth.) **225**, 184 (2007).

[30] A. A. Kistanov, R. T. Murzaev, S. V. Dmitriev, V. I. Dubinko, and V. V. Khizhnyakov, Moving discrete breathers in a monoatomic two-dimensional crystal, JETP Lett. **99**, 353 (2014).

[31] E. A. Korznikova, S. Yu. Fomin, E. G. Soboleva, and S. V. Dmitriev, Highly symmetric discrete breather in a two-dimensional Morse crystal, JETP Lett. **103**, 277 (2016).

[32] R. I. Babicheva, A. S. Semenov, E. G. Soboleva, A. A. Kudreyko, K. Zhou, and S. V. Dmitriev, Discrete breathers in a triangular β-Fermi-Pasta-Ulam-Tsingou lattice, Phys. Rev. E **103**, 052202 (2021).

[33] S. V. Dmitriev, E. A. Korznikova, D. I. Bokij, and K. Zhou, Auxeticity from nonlinear vibrational modes, Phys. Status Solidi B **253**, 1310 (2016).

[34] V. M. Burlakov and S. Kiselev, Molecular-dynamics simulation of the decay kinetics of uniform excitation of an anharmonic 1D chain, Zh. Eksp. Teor. Fiz. **99**, 1526 (1991) [Sov. Phys. JETP **72**, 854 (1991)].

[35] V. V. Mirnov, A. J. Lichtenberg, and H. Guclu, Chaotic breather formation, coalescence, and evolution to energy equipartition in an oscillatory chain, Phys. D (Amsterdam, Neth.) **157**, 251 (2001).

[36] K. Ullmann, A. J. Lichtenberg, and G. Corso, Energy equipartition starting from high-frequency modes in the Fermi–Pasta–Ulam β oscillator chain, Phys. Rev. E **61**, 2471 (2000).

[37] Y. A. Kosevich and S. Lepri, Modulational instability and energy localization in anharmonic lattices at finite energy density, Phys. Rev. B **61**, 299 (2000).

[38] T. Cretegny, T. Dauxois, S. Ruffo, and A. Torcini, Localization and equipartition of energy in the β-FPU chain: Chaotic breathers, Phys. D (Amsterdam, Neth.) **121**, 109 (1998).

[39] B. Tang and K. Deng, Discrete breathers and modulational instability in a discrete ϕ^4 nonlinear lattice with next-nearest-neighbor couplings, Nonlinear Dyn. **88**, 2417 (2017).

[40] E. A. Korznikova, D. V. Bachurin, S. Yu. Fomin, A. P. Chetverikov, and S. V. Dmitriev, Instability of vibrational modes in hexagonal lattice, Eur. Phys. J. B **90**, 23 (2017).

[41] L. Kavitha, A. Mohamadou, E. Parasuraman, D. Gopi, N. Akila, and A. Prabhu, Modulational instability and nano-scale energy localization in ferromagnetic spin chain with higher order dispersive interactions, J. Magn. Magn. Mat. **404**, 91 (2016).

[42] L. Kavitha, E. Parasuraman, D. Gopi, A. Prabhu, and R. A. Vicencio, Nonlinear nano-scale localized breather modes in a discrete weak ferromagnetic spin lattice, J. Magn. Magn. Mat. **401**, 394 (2016).

[43] A. Upadhyaya, M. N. Semenova, A. A. Kudreyko, and S. V. Dmitriev, Chaotic discrete breathers and their effect on macroscopic properties of triangular lattice, Commun. Nonlinear Sci. Numer. Simul. **112**, 106541 (2022).

[44] P. M. Morse, Diatomic molecules according to the wave mechanics. II. Vibrational levels, Phys. Rev. **34**, 57 (1929).

[45] L. A. Girifalco and G. V. Weizer, Application of the Morse potential function to cubic metals, Phys. Rev. **114**, 687 (1959).

[46] N. S. Bakhvalov, *Numerical Methods: Analysis, Algebra, Ordinary Differential Equations* (MIR, Moscow, 1977).

[47] G. H. Golub and H. A. van der Vorst, Eigenvalue computation in the 20th century, J. Comput. Appl. Math. **123**, 35 (2000).

[48] X. W. Zhou, H. N. G. Wadley, R. A. Johnson, D. J. Larson, N. Tabat, A. Cerezo, A. K. Petford-Long, G. D. W. Smith, P. H. Clifton, R. L. Martens, and T. F. Kelly, Atomic scale structure of sputtered metal multilayers, Acta Mater. **49**, 4005 (2001).

[49] S. V. Dmitriev, Discrete breathers in crystals: Energy localization and transport, J. Micromechan. Mol. Phys. **01**, 1630001 (2016).

[50] V. A. Kuzkin and A. M. Krivtsov, Nonlinear positive/negative thermal expansion and equations of state of a chain with longitudinal and transverse vibrations, Phys. Status Solidi (B) **252**, 1664 (2015).

[51] M. B. Babenkov, A. M. Krivtsov, and D. V. Tsvetkov, Energy oscillations in a one-dimensional harmonic crystal on an elastic substrate, Phys. Mesomechan. **19**, 282 (2016).

[52] A. A. Sokolov, A. M. Krivtsov, and W. H. Müller, Localized heat perturbation in harmonic 1D crystals: Solutions for the equation of anomalous heat conduction, Phys. Mesomechan. **20**, 305 (2017).